Highly efficient Förster resonance energy transfer between emissive tetraphenylethylene-based metal–organic cage and the encapsulated dye guest

Danyang Li, [a] Xin Liu, [a] Linlin Yang, [b] Hechuan Li, [a] Guoxu Guo, [a] Xuezhao Li [a] and Cheng He * [a]

[a]*State Key Laboratory of Fine Chemicals, Dalian University of Technology, Dalian, 116023, P. R. China.*

[b]*Xinxiang Key Laboratory of Forensic Science Evidence, School of Forensic Medicine, Xinxiang Medical University, Xinxiang 453003, P. R. China.*

*Correspondence authors.

E-mail: hecheng@dlut.edu.cn

Table of Contents

1 Measurements and Materials

1.1 Materials.

5-Nitro-2, 2'-bipyridine (1), 5-Amino-2, 2'-dipyridine (2), Tetrakis(4-bromophenyl)ethene (3), Tetrakis(4-cyanophenyl)ethylene (4), Tetrakis(4-carboxyphenyl)ethylene (5) were synthesized according to published procedures [S1, S2]. 2-Bromo-5-nitropyridine, 2-(tributylstannyl)pyridine, 10 % Pd/C, sodium borohydride, tetraphenylethylene, bromine, Copper(I) cyanide, ethylene glycol, hydrochloric acid, ethylenediamine, potassium hydroxide, thionyl chloride, triethylamine, Zinc tetrafluoroborate ($Zn(BF_4)_2$) were all obtained from commercial sources and used as received. Unless stated otherwise, all operations were carried out under an atmosphere of dry argon using Schlenk and vacuum techniques. Solvents were dried by standard methods and freshly distilled prior to use.

1.2 Measurements.

^{1}H NMR spectra were measured on a Varian DLG 400M and Bruker Avance 500M spectrometer. Electrospray ionization mass spectrometry (ESI-MS) measurements were carried out on HPLC-Q-Tof MS spectrometer. UV-Vis spectra were measured on HP 8453 spectrometer. The fluorescent experiments were measured on Edinburgh FS-920 and FLS 1000. Gas Chromatography analysis was performed on an Agilent 6890N instrument equipped with a HP-5 capillary column (30 m × 0.32 mm × 0.25 μm) and FID detector. Isothermal Titration Calorimetry (ITC) were performed on a Nano ITC (TA Instruments Inc. -Waters LLC).

1.3 Preparation and characterizations.

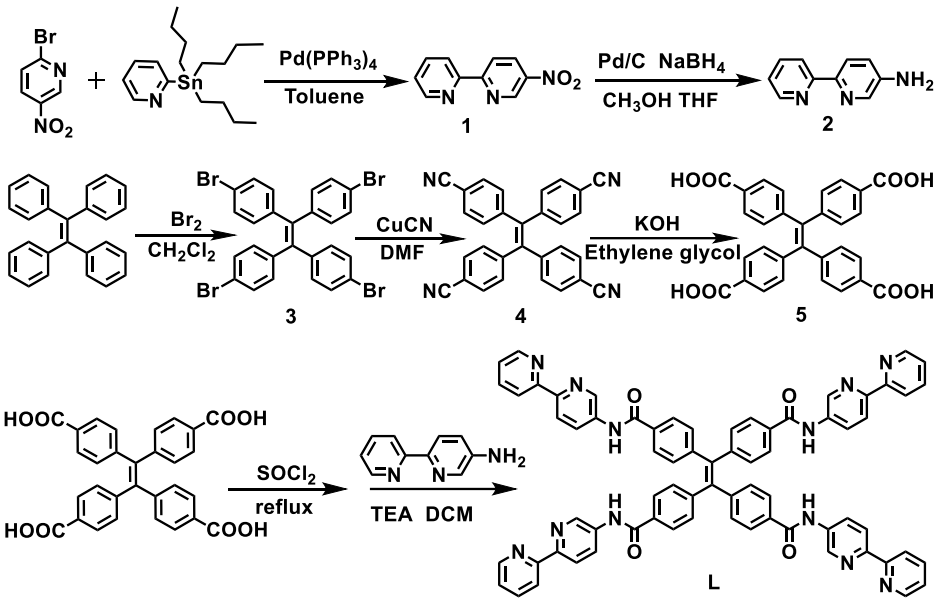

Scheme S1. The synthetic routes of the ligand **L**.

5-Nitro-2, 2'-dipyridine (1). A mixture of 2-Bromo-5-nitropyridine (2.56 g, 12.60 mmol), anhydrous toluene (200 mL) and 2-(tributylstannyl)pyridine (4.37 mL, 13.60 mmol) was degassed with argon for 20 min, $Pd(PPh_3)_4$ (0.50 g, 0. 25 mmol) was added into the mixture. The reaction mixture was degassed and heated at reflux under argon for 3 days. The mixture was allowed to cool to room temperature. The precipitated residue was filtered off. The filtrate was extracted with DCM, dried over $MgSO_4$ and subsequently evaporated under vacuum. The residue was purified by silica gel column chromatography (dichloromethane/PE = 2:1 v/v) to give compound 1 as a white soild (1.78g, 70%)

^{1}H NMR (400 MHz, $CDCl_3$): δ 9.46 (dd, J = 2.6, 0.7 Hz, 1H), 8.77-8.70 (m, 1H), 8.64 (s, 1H), 8.57 (d, J = 2.6 Hz, 1H), 8.51 (s, 1H), 7.88 (dd, J = 7.8, 1.8 Hz, 1H), 7.40 (dd, J = 4.8, 1.2 Hz, 1H).

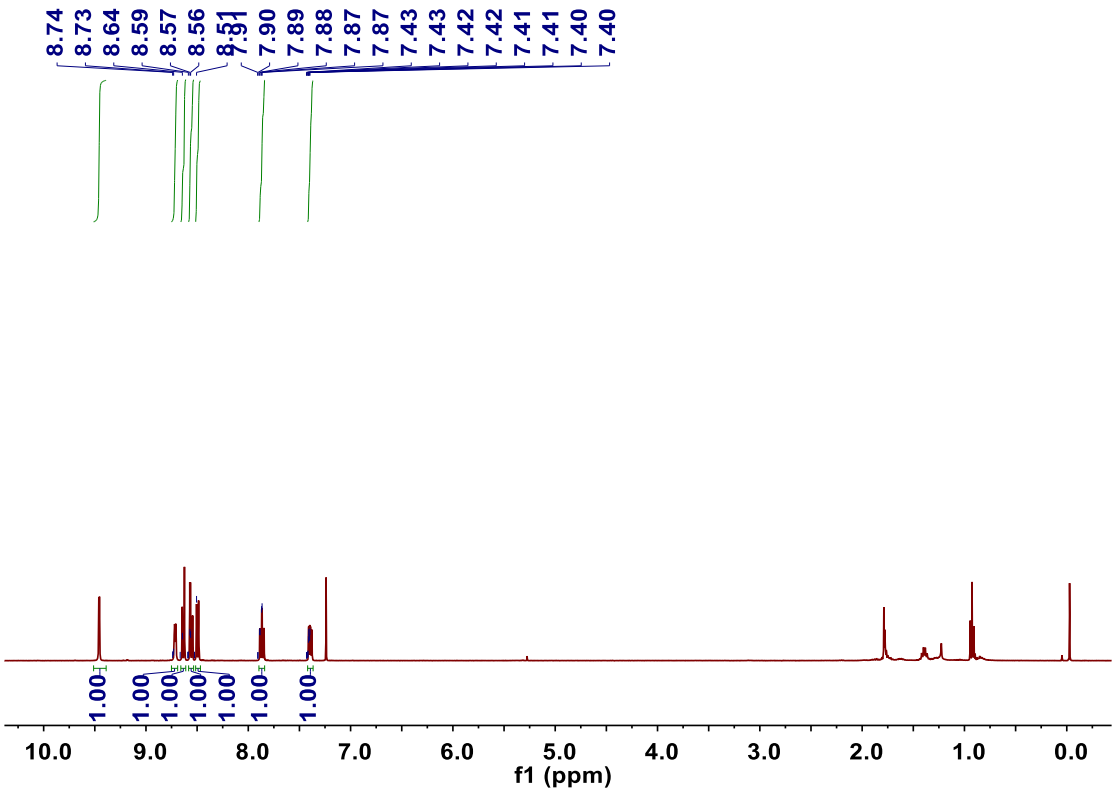

Figure S1. ^{1}H NMR spectrum (400 MHz, $CDCl_3$) of 5-Nitro-2, 2'-dipyridine(1).

5-Amino-2, 2'-dipyridine (2). The suspension of **1** (2.50 g, 12.40 mmol) and 10 % Pd/C (0.60 g) were dissolved in anhydrous CH_3OH (180 mL) and THF (120ml). The system was degassed with argon for 10 min and heated to 45 °C until completely dissolved. Then $NaBH_4$ (8.00 g, 212 mmol) was added in batches. The reaction mixture was stirred at room temperature for 6 h. After the reaction was over, the mixture was filtered through celite and washed with DCM. The filtrate was collected and removed under vacuum. The resulting solid was extracted with DCM, dried over $MgSO_4$ and the solvent was removed under vacuum. The white solid product was produced. Yield: 1.74 g (82%).

^{1}H NMR (400 MHz, $CDCl_3$): δ 8.61 (d, J = 4.7 Hz, 1H), 8.24 (d, J = 8.0 Hz, 1H), 8.19 (d, J = 8.5 Hz, 1H), 8.15 (d, J = 2.7 Hz, 1H), 7.74 (t, J = 7.2 Hz, 1H), 7.23 - 7.17 (m, 1H), 7.09 (dd, J = 8.5, 2.5 Hz, 1H), 3.83 (s, 2H).

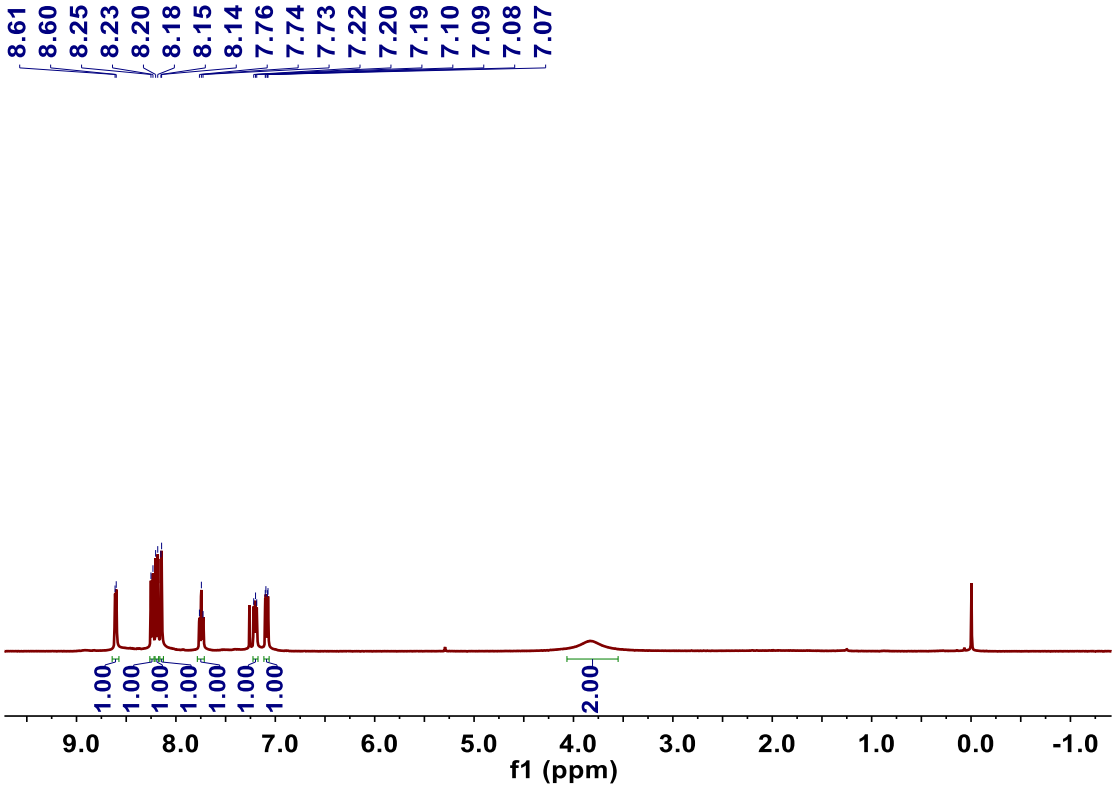

Figure S2. ^{1}H NMR spectrum (400 MHz, $CDCl_3$) of 5-Amino-2, 2'-dipyridine(2).

Tetrakis(4-bromophenyl)ethene (3). Bromine (18 mL) was dripped into the mixture of tetraphenylethylene (9.96 g, 30.00 mmol, 1.00 equiv.) and CH_2Cl_2 (500 mL) at 0 °C using an ice water bath, and the mixture was allowed to warm to room temperature and stir at room temperature for 14 h. The reaction mixture was washed with saturated aq. Na_2SO_3 (200 mL), saturated aq. Na_2CO_3 (200 mL), brine (200 mL) and dried over $MgSO_4$. The solvent was removed under reduced pressure to yield an off-white solid. This solid was washed with n-hexane (50 mL) and filtered to obtain a white solid, yielding a white solid (18.30 g, 94%).

^{1}H NMR (400 MHz, $CDCl_3$): δ 7.24 (d, J = 3.0 Hz, 1H), 6.83 (d, J = 8.6 Hz, 1H). This spectrum is consistent with that reported in the literature.

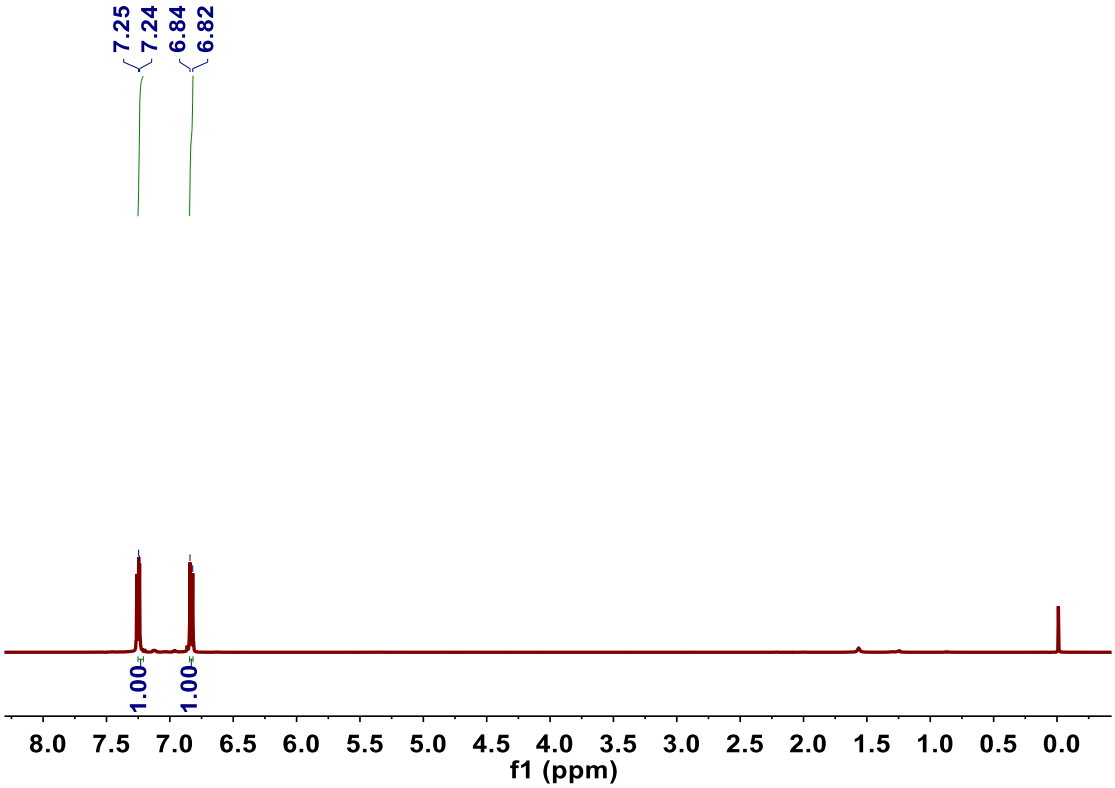

Figure S3. ^{1}H NMR spectrum (400 MHz, $CDCl_3$) of Tetrakis(4-bromophenyl)ethene (3).

Tetrakis(4-cyanophenyl)ethylene (4). A mixture of **3** (3.00 g, 4.63 mmol) and Copper(I) cyanide (2.37 g, 26.40 mmol) in dry DMF (45 mL) was degassed with argon for 20 min, then heated at reflux under argon for 3 days. Water (15 mL) and ethylenediamine (10 mL) were added to the reaction mixture after they had cooled to 90 °C. The resulting mixture was stirred at 90 °C for 3 h and then cooled to room temperature. The product was extracted with DCM and the organic layer dried over $MgSO_4$, filtered, and evaporated. The yellow crude product 1.16 g (56% yield) without further purified for the next step.

Tetrakis(4-carboxyphenyl)ethylene (5). A mixture of KOH (5.50 g, 98.00 mmol) and **4** (4.11 g, 9.50 mmol) was refluxed for 3 days in ethylene glycol (300 mL). After cooling to room temperature, distilled water (150 mL) was added to the mixture. The mixture was washed with DCM. The aqueous/ethylene glycol fraction was acidified using hydrochloric acid (1 M) and the yellow precipitate was washed with water and DCM. The residue was then recrystallized from DCM/ethanol mixture to afford a pale yellow powder 3.40 g (70 % yield).

^{1}H NMR (400 MHz, DMSO-d$_6$): δ 12.93 (s, 1H), 7.74 (d, J = 8.3 Hz, 2H), 7.11 (d, J = 8.3 Hz, 2H).

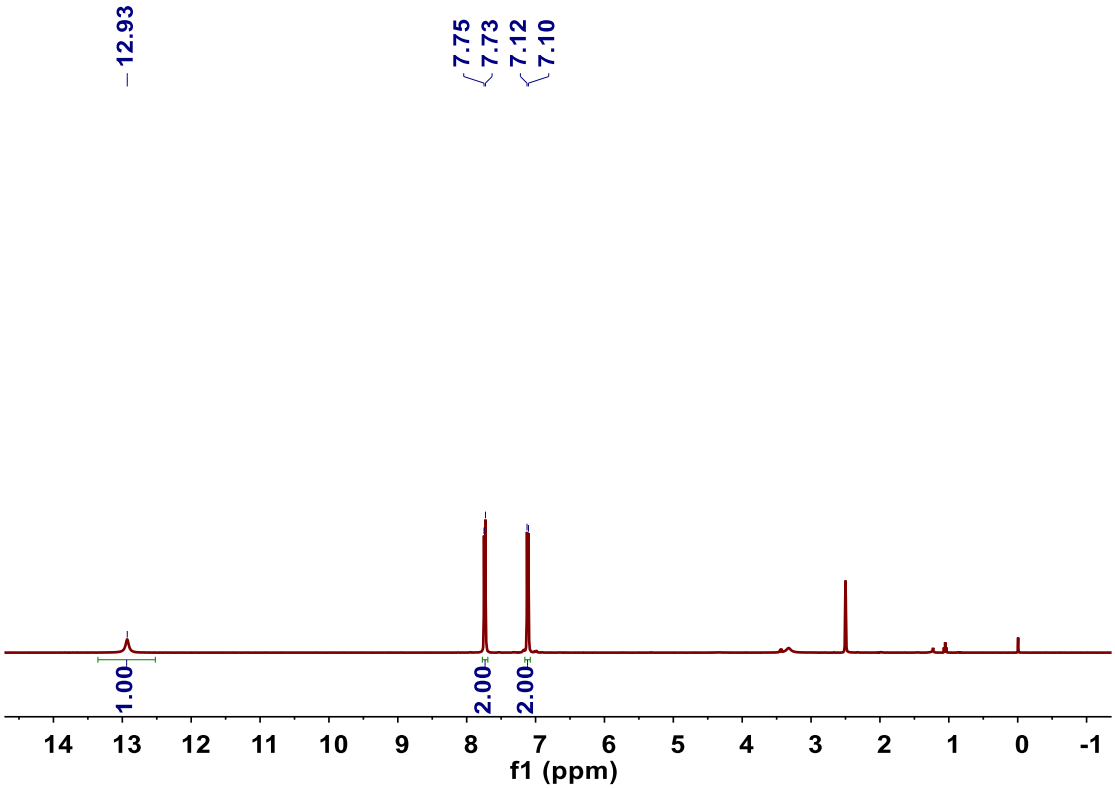

Figure S4. ^{1}H NMR spectrum (400 MHz, DMSO-d$_6$) of Tetrakis(4-carboxyphenyl)ethylene (5).

4,4',4'',4'''-(ethene-1,1,2,2-tetrayl)tetrakis(N-([2,2'-bipyridin]-5-yl)benzamide)(L). Under the anhydrous atmosphere, a mixture of **5** (0.60 g, 1.18 mmol) in $SOCl_2$ (15 mL) was stirred at 80 ^oC for 12 h. The reaction vessel was cooled to room temperature and the solvents were removed under vacuum. The resulting solid was then dissolved in anhydrous DCM (30 mL), which was gradually added to a solution of **2** (1.21 g, 7.08 mmol), triethylamine (3 mL) in anhydrous DCM (30 mL). The suspension was stirred at room temperature for 4 days. Then the precipitate was collected, washed with water, DCM. Subsequent drying under high vacuum led to **L** as a pale yellow solid. Yield: 620mg (46.9%). Anal. Calcd for $C_{70}H_{48}N_{12}O_4$: C, 74.97; H, 0.04; N, 0.15. Found: C, 74.10; H, 0.04; N, 0.14.

^{1}H NMR (400 MHz, DMSO-d$_6$): δ 10.61 (s, 1H), 9.05 (s, 1H), 8.67 (s, 1H), 8.37 (s, 3H), 7.90 (s, 3H), 7.44 (s, 1H), 7.28 (s, 2H).

^{13}C NMR (126 MHz, DMSO-d$_6$): δ 165.39, 155.02, 150.31, 149.17, 145.83, 141.27, 137.17, 136.23, 132.81, 130.81, 130.75, 127.90, 127.77, 123.63, 120.39, 119.98

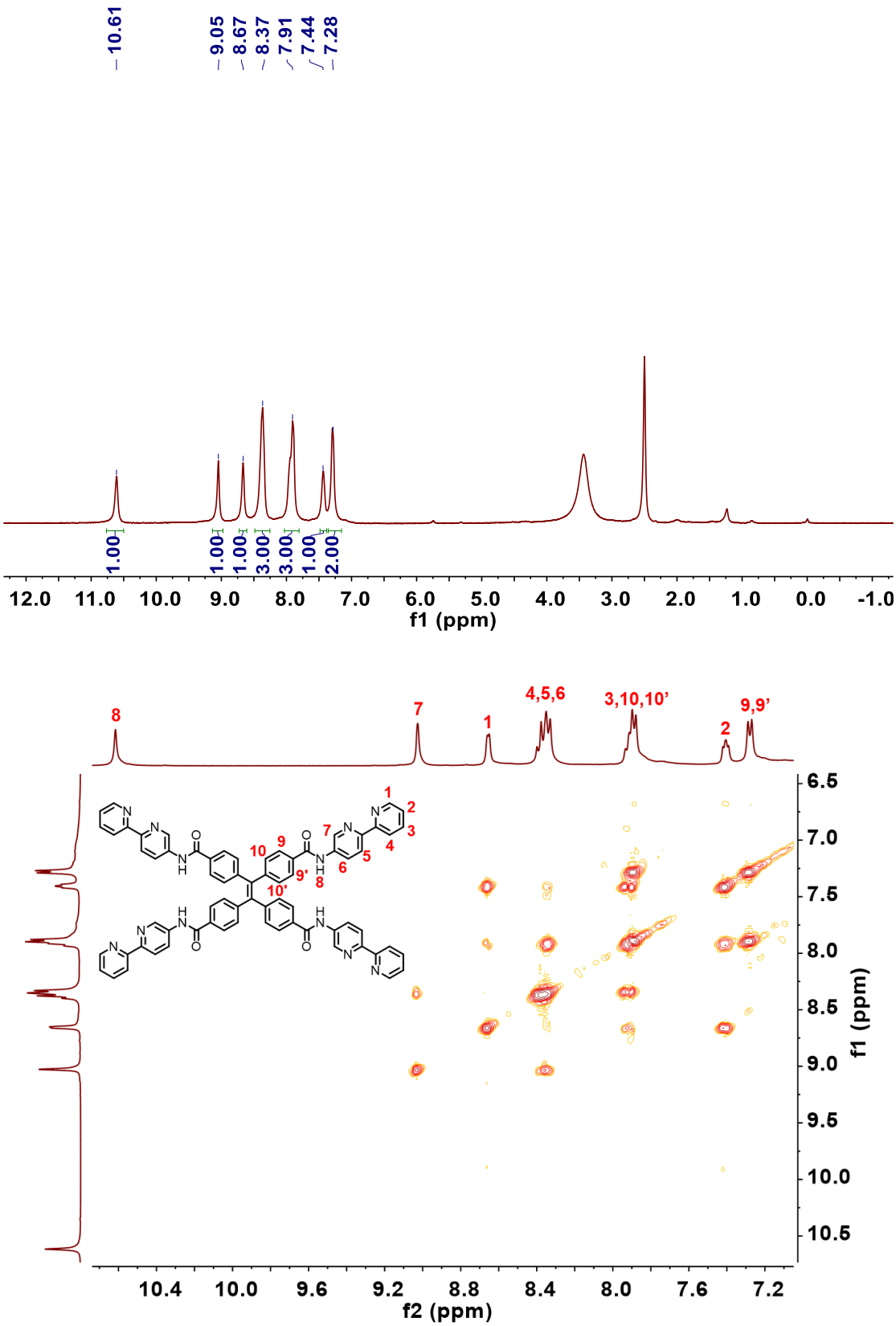

Figure S5. ^{1}H NMR (DMSO-d_6) and ^{1}H -^{1}H COSY spectrum of **L**.

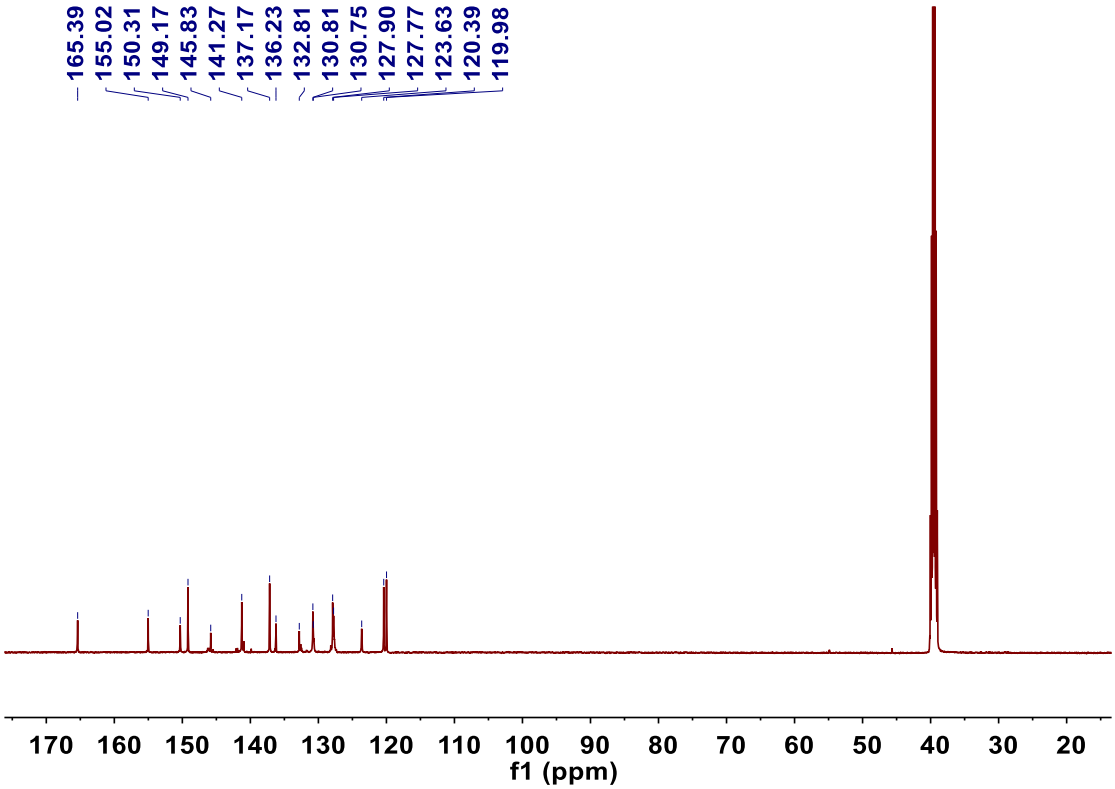

Figure S6. ^{13}C NMR (126 MHz, DMSO-d_6) spectrum of **L**.

Synthesis of the cage Zn-1

A mixture of **L** (101.00 mg, 0.09 mmol) and Zinc tetrafluoroborate (28.60 mg, 0.12 mmol) was dissolved in 30 mL DMF. The reaction mixture was heated at 80 °C for 12 hours. This solution was added to diethyl ether and the product was obtained after centrifugation and then dried. The desired product was obtained as a light brown solid 61 % yield (based on the solid dried in vacuum).

^{1}H NMR (400 MHz, DMSO-d$_6$): δ 10.77 (s, 1H), 8.81 (d, J = 100.9 Hz, 3H), 8.49 – 7.98 (m, 3H), 7.59 (d, J = 69.5 Hz, 3H), 7.06 (d, J = 28.4 Hz, 2H).

^{13}C NMR (126 MHz, DMSO-d$_6$): δ 167.48, 149.37, 148.51, 146.95, 146.50, 144.39, 142.90, 140.68, 140.15, 137.67, 133.61, 131.59, 128.45, 127.98, 124.87, 123.75.

^{19}F NMR (CD$_3$CN, 400 MHz): δ -148.19.

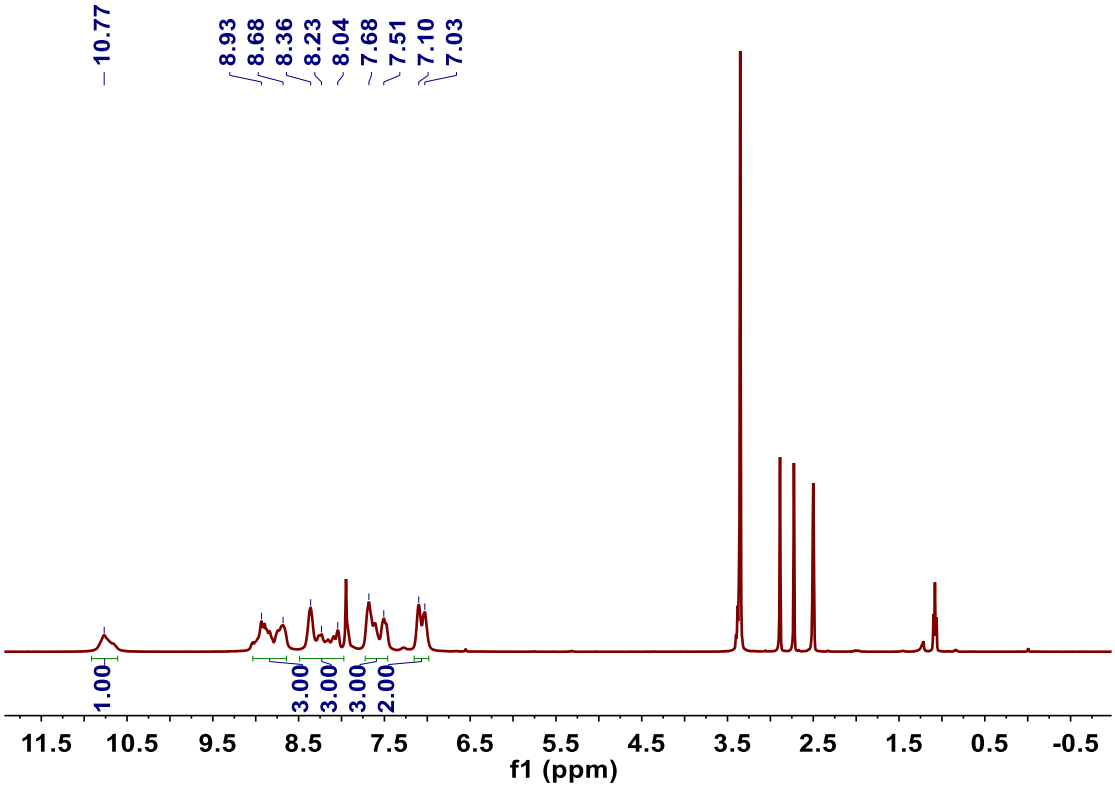

Figure S7. ^{1}H NMR (DMSO-d$_6$) spectrum of **Zn-1**.

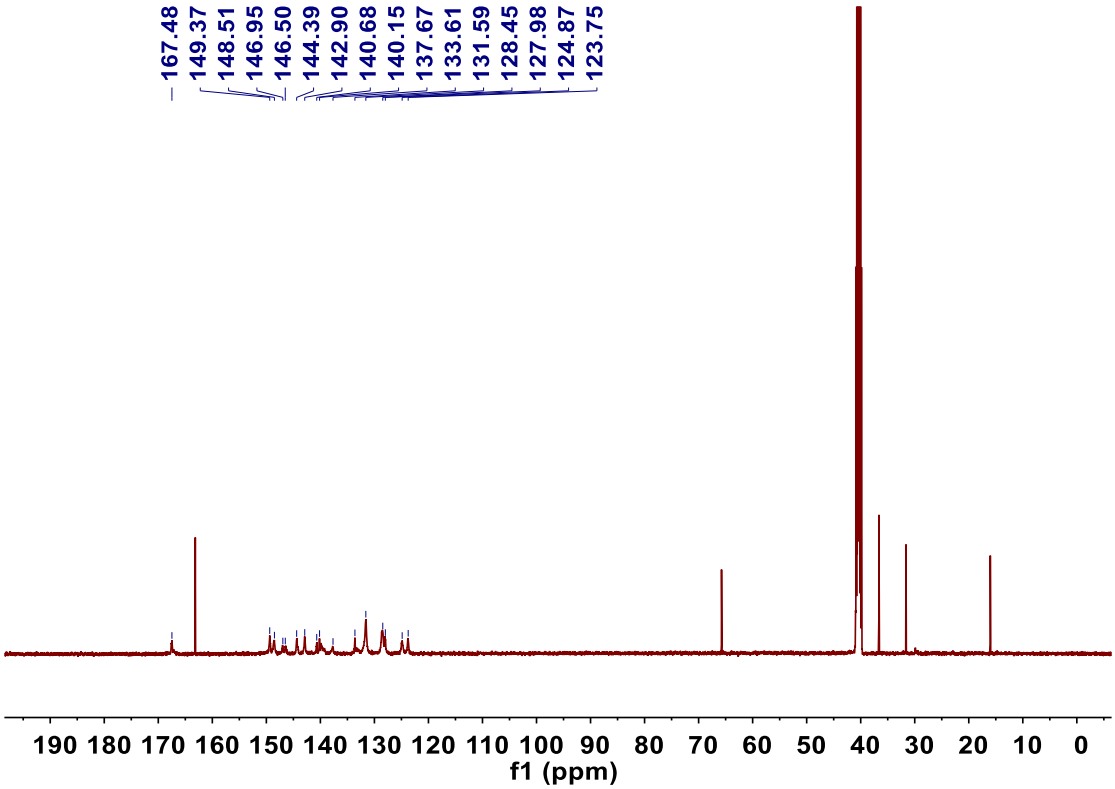

Figure S8. ^{13}C NMR (126 MHz, DMSO-d_6) spectrum of **Zn-1**.

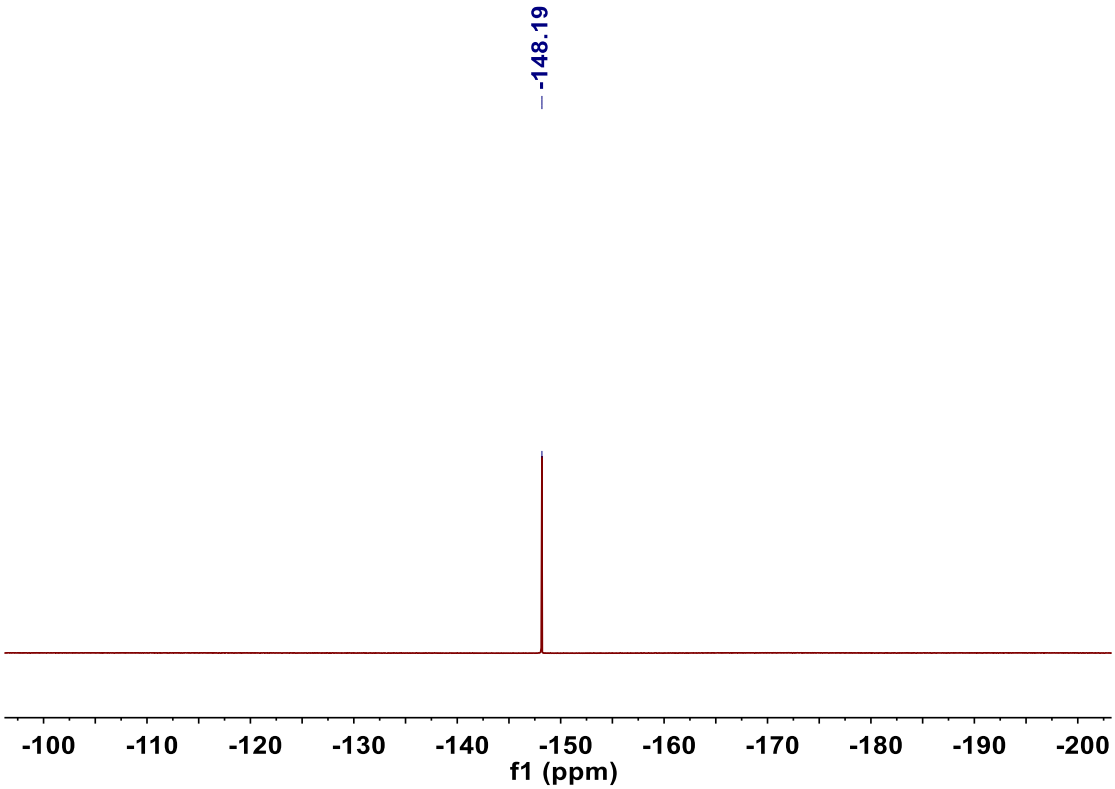

Figure S9. ^{19}F NMR spectrum of **Zn-1**.

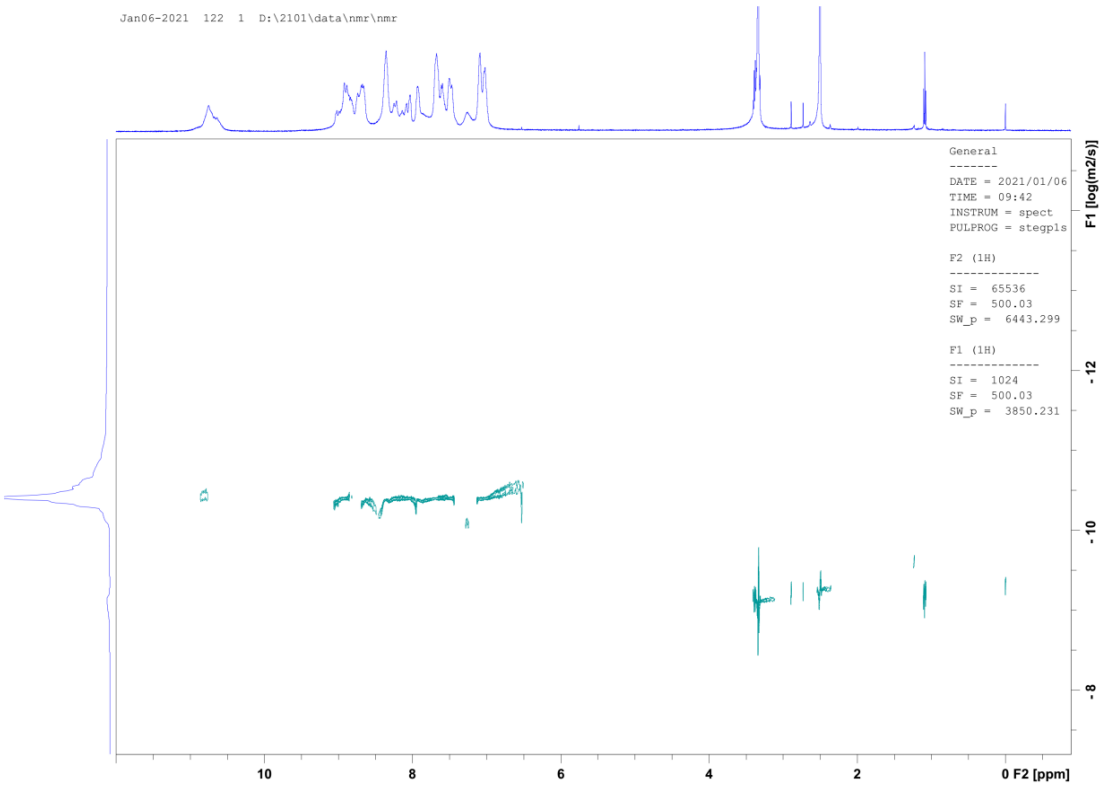

Figure S10. DOSY spectrum of **Zn-1** in DMSO-d_6.

2 Crystallography

Intensities of single crystals were collected on a Bruker D8-Venture diffractometer equipped with graphite monochromated Mo-Kα (λ = 0.71073 Å) using the SMART and SAINT programs.[S3, S4] The structure was solved by direct methods and refined on F^2 by full-matrix least-squares methods with SHELXTL-2018 version software.[S5]

In the structural refinement of **Zn-1**, except the disordered part in the ligands, the BF_4^- anions and the solvent molecules, the other non-hydrogen atoms were refined anisotropically. Hydrogen atoms were fixed geometrically at calculated distances and allowed to ride on the parent of the non-hydrogen atoms on the ligands. The skeleton ligands and the anions were almost disordered and divided into two parts with the site occupied factor (*s.o.f.)* of each part being fix on suitable values. To assist the stability of refinements of the huge structure, a lot of restrains were applied: (1) Many of the respective bond distances in the ligands and the anions were restrained to the idealized values; (2) Geometrical constraints of idealized regular polygons for some disordered rings in the ligands and the anions were used; (3) Thermal parameters on adjacent atoms in the some of the disordered parts were restrained to be similar. And the highly disordered state of some BF_4^- anions and the incorporated molecule solvents meant that they could not be located, and hence in the final refinement, the electron density was treated with the SQUEEZE routine in the PLATON program package.

In the structural refinement of **Zn-1⊃EY**, except the partly occupied atoms, the other non-hydrogen atoms were refined anisotropically. Hydrogen atoms were fixed geometrically at calculated distances and allowed to ride on the parent of the non-hydrogen atoms on the ligands and **EY**. Also, the skeleton ligands and the anions were almost disordered and divided into two parts with the site occupied factor (*s.o.f.)* of each part being fix on suitable values. To assist the stability of refinements of the huge structure, a lot of restrains were applied: (1) Many of the respective bond distances in **EY**, the ligands and the anions were restrained to the idealized values; (2) Geometrical constraints of idealized regular polygons for the anions, the aromatic rings **EY** and some disordered rings in the ligands were used; (3) Thermal parameters on adjacent

atoms in the some of the disordered parts in ligands and **EY** were restrained to be similar. And the highly disordered state of some BF_4^- anions and the incorporated molecule solvents meant that they could not be located, and hence in the final refinement, the electron density was treated with the SQUEEZE routine in the PLATON program package.

In the checkcif results of the crystal data, the A alert was caused by the weak diffraction intensity. Due to poor quality of the crystals, and the presence of larger number of atoms in the asymmetrical units as well as the highly disordered state of the components, some of the refinement results is not well agree with ideal value.

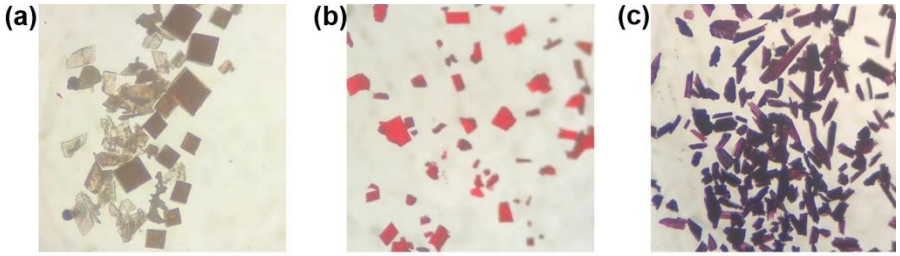

Figure S11. Pictures of solid crystal (a) **Zn-1**; (b) **Zn-1⊃EY**; (c) **Zn-1⊃ SR101**, rendered under microscope.

Table S1. Selective bond distance (Å) in **Zn-1**.

	bond distance (Å)		bond distance (Å)
Zn1—N407	2.108 (4)	Zn5—N202	2.103 (5)
Zn1—N307	2.112 (5)	Zn5—N102	2.125 (5)
Zn1—N501	2.133 (5)	Zn5—N404	2.133 (5)
Zn1—N408	2.137 (4)	Zn5—N201	2.149 (5)
Zn1—N308	2.155 (4)	Zn5—N405	2.162 (5)
Zn1—N502	2.178 (4)	Zn5—N101	2.174 (10)
Zn2—N107	2.087 (5)	Zn6—N204	1.984 (5)
Zn2—N607	2.127 (5)	Zn6—N401	2.064 (6)
Zn2—N108	2.140 (5)	Zn6—N205	2.152 (5)
Zn2—N608	2.149 (6)	Zn6—N305	2.191 (5)
Zn2—N508	2.149 (4)	Zn6—N402	2.194 (5)
Zn2—N507	2.159 (4)	Zn6—N304	2.199 (5)
Zn3—N105	2.030 (5)	Zn7—N211	2.012 (7)
Zn3—N410	2.087 (5)	Zn7—N210	2.065 (8)
Zn3—N505	2.116 (5)	Zn7—N611	2.082 (6)
Zn3—N104	2.171 (5)	Zn7—N110	2.102 (3)
Zn3—N411	2.172 (4)	Zn7—N111	2.110 (3)
Zn3—N504	2.180 (5)	Zn7—N610	2.172 (7)
Zn4—N605	2.113 (5)	Zn8—N602	1.970 (5)
Zn4—N301	2.117 (5)	Zn8—N601	1.998 (11)
Zn4—N207	2.131 (6)	Zn8—N510	2.030 (6)
Zn4—N302	2.149 (5)	Zn8—N310	2.038 (7)
Zn4—N604	2.184 (5)	Zn8—N311	2.088 (6)
Zn4—N208	2.188 (4)	Zn8—N511	2.130 (6)

Table S2. Selective bond distance (Å) in **Zn-1⊃EY**.

	bond distance (Å)		bond distance (Å)
Zn1—N304	2.163(4)	Zn5—N207	2.173(4)
Zn1—N305	2.161(3)	Zn5—N208	2.127(7)
Zn1—N401	2.118(3)	Zn5—N311	2.115(4)
Zn1—N402	2.180(3)	Zn5—N310	2.003(7)
Zn1—N504	2.172(3)	Zn5—N610	2.156(5)
Zn1—N505	2.120(3)	Zn5—N611	2.154(4)
Zn2—N204	2.137(4)	Zn6—N107	2.144(4)
Zn2—N205	2.176(4)	Zn6—N108	2.170(4)
Zn2—N307	2.109(4)	Zn6—N410	2.139(4)
Zn2—N308	2.168(3)	Zn6—N411	2.157(4)
Zn2—N501	2.159(4)	Zn6—N507	2.178(5)
Zn2—N502	2.119(3)	Zn6—N508	2.167(5)
Zn3—N104	2.163(4)	Zn7—N110	2.122(5)
Zn3—N105	2.136(4)	Zn7—N111	2.137(4)
Zn3—N201	2.135(4)	Zn7—N407	2.173(5)
Zn3—N202	2.147(4)	Zn7—N408	2.150(5)
Zn3—N510	2.144(4)	Zn7—N604	2.160(5)
Zn3—N511	2.156(4)	Zn7—N605	2.170(5)
Zn4—N101	2.135(4)	Zn8—N301	2.125(5)
Zn4—N102	2.140(4)	Zn8—N302	2.136(4)
Zn4—N211	2.184(6)	Zn8—N404	2.171(6)
Zn4—N210	2.020(6)	Zn8—N405	2.265(6)
Zn4—N601	2.147(5)	Zn8—N607	1.977(7)
Zn4—N602	2.130(5)	Zn8—N608	1.819(7)

3 Theoretical Methods

Theoretical calculations were performed to obtain the encapsulation structure of **SR101** into **Zn-1** cage. We started with **Zn-1** cage from crystallography results, containing 8 Zn ions carrying +16 charges. The freestanding **Zn-1** cage was firstly optimized with semi-empirical PM-7 method[S6] as implemented in Gaussian 16 Rev A03,[S7] considering there are 812 atoms in the freestanding **Zn-1** cage. Electronic structure of freestanding **SR101** was then investigated with full-electron Gaussian-type basis sets developed by Collins and Hehre for C, N, H, S and O atoms[S8, S9] and B3LYP functional[S10, S11]. With the optimized structures of **Zn-1** cage, **SR101** the encapsulation structure was obtained by structural relaxations on structures constructed by placing the **SR101** guest of various conformations at various positions in the **Zn-1** cage. The most plausible structure was considered for the subsequent analysis.

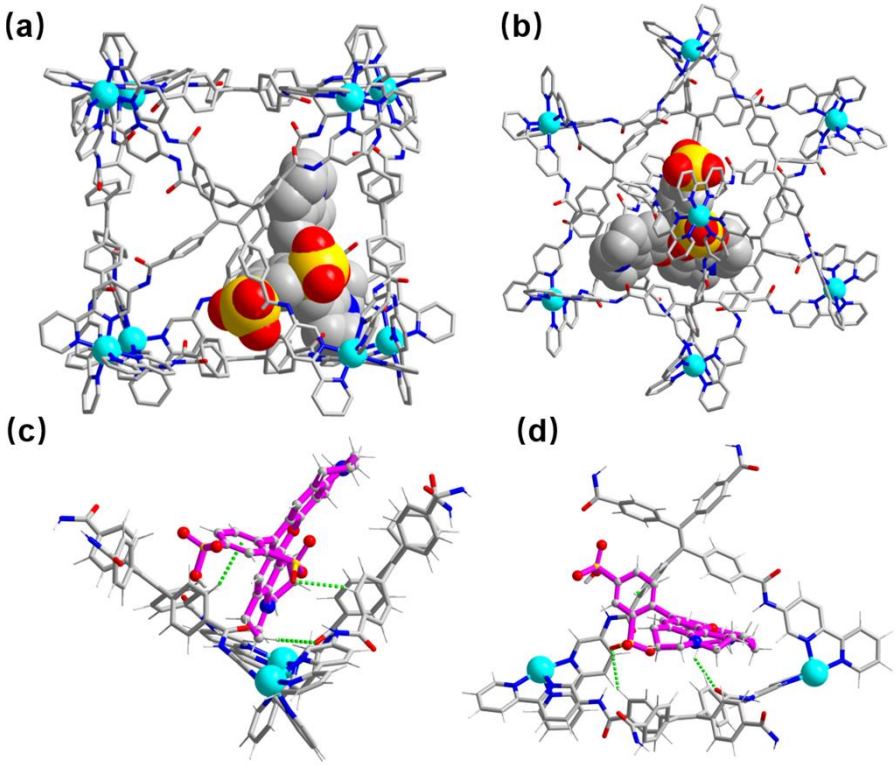

Figure S12. (a), (b) Representation of the optimized structure of **Zn-1** with one **SR101** from different directions (the cavity-bound guest **SR101** shows space-filling); (c), (d) the different views showing C–H···π and C–H···O interactions between **SR101** and **Zn-1**. Color coding: Zn = cyan; C = gray; N = blue; O = red; S = yellow.

4 Host-Guest Complexes with Encapsulation of EY and SR101.

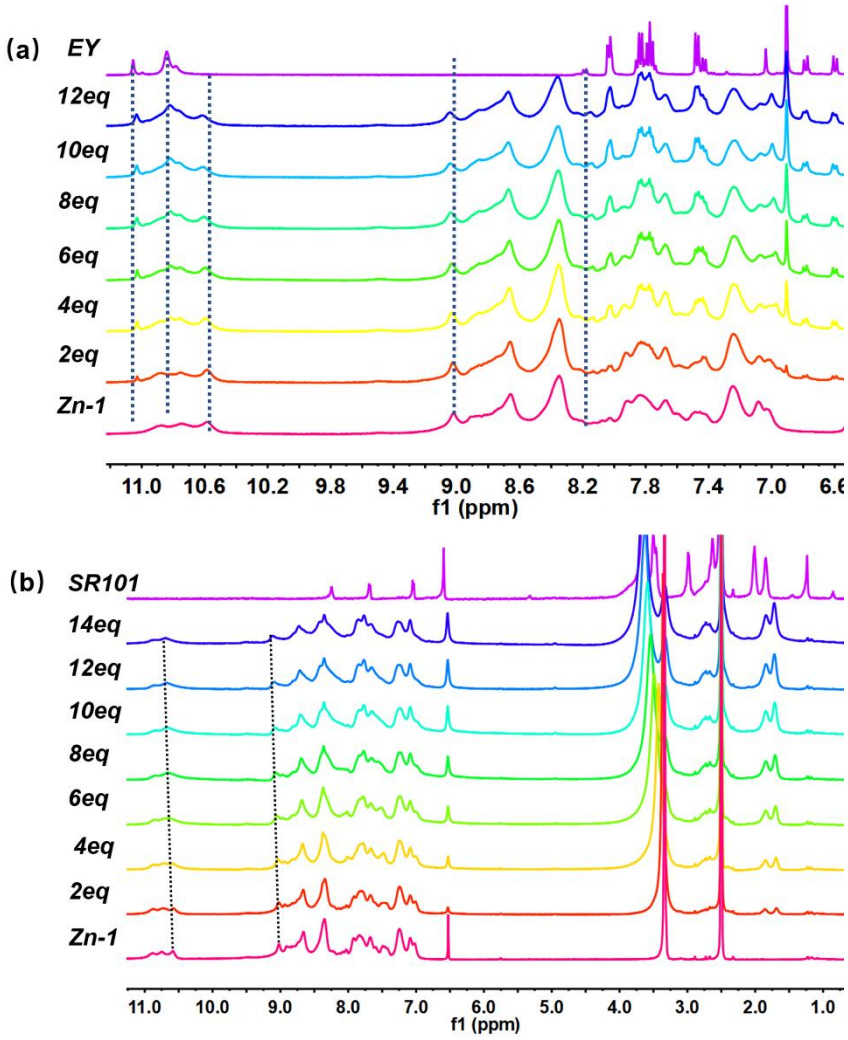

Figure S13. (a)^{1}H NMR titration (400 MHz, DMSO-d_6) of **Zn-1** titrated by **EY**; (b) ^{1}H NMR titration (400 MHz, DMSO-d_6) of **Zn-1** titrated by **SR101**.

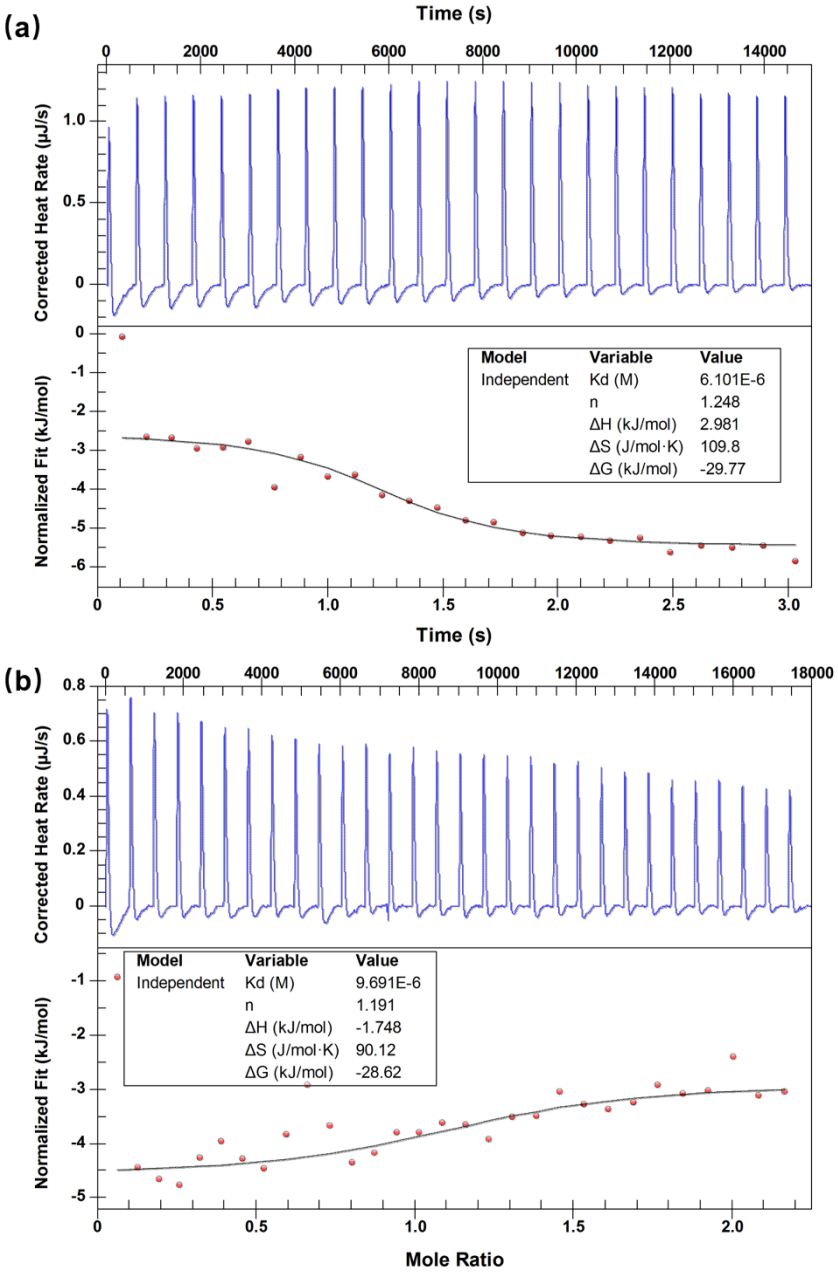

Figure S14. (a) Microcalorimetric titration of **Zn-1** with **EY** in DMF solution at 298.15 K. (Top) Raw data for sequential 25 injections (10 µL per injection) of **EY** solution (1.0 mM) injecting into **Zn-1** solution (0.1 mM). (Bottom) Apparent reaction heat obtained from the integration of calorimetric traces; (b) microcalorimetric titration of **Zn-1** with **SR101** in DMF solution at 298.15 K. (Top) Raw data for sequential 30 injections (8 µL per injection) of **SR101** solution (0.9 mM) injecting into **Zn-1** solution (0.12 mM). (Bottom) Apparent reaction heat obtained from the integration of calorimetric traces.

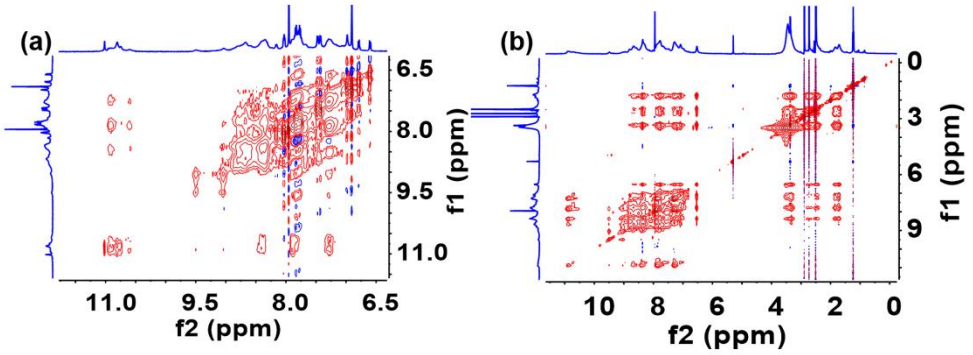

Figure S15. NOE spectrum of (a) **Zn-1⊃EY**; (b) **Zn-1⊃SR101** in DMSO-d_6.

5 Photophysical Properties.

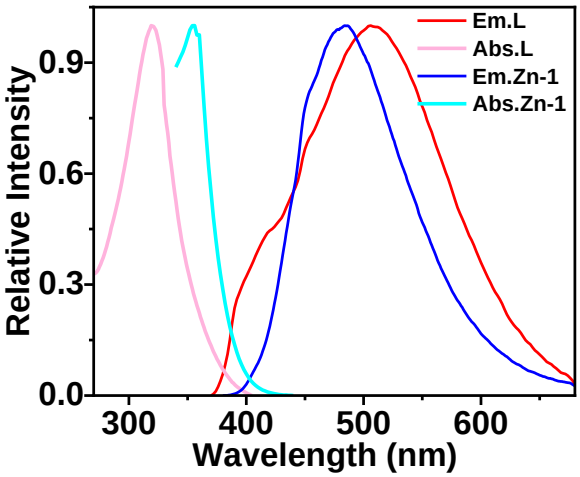

Figure S16. UV-Vis absorption and fluorescence spectra of **Zn-1** (cyan and blue line) and **L** (pink and red line).

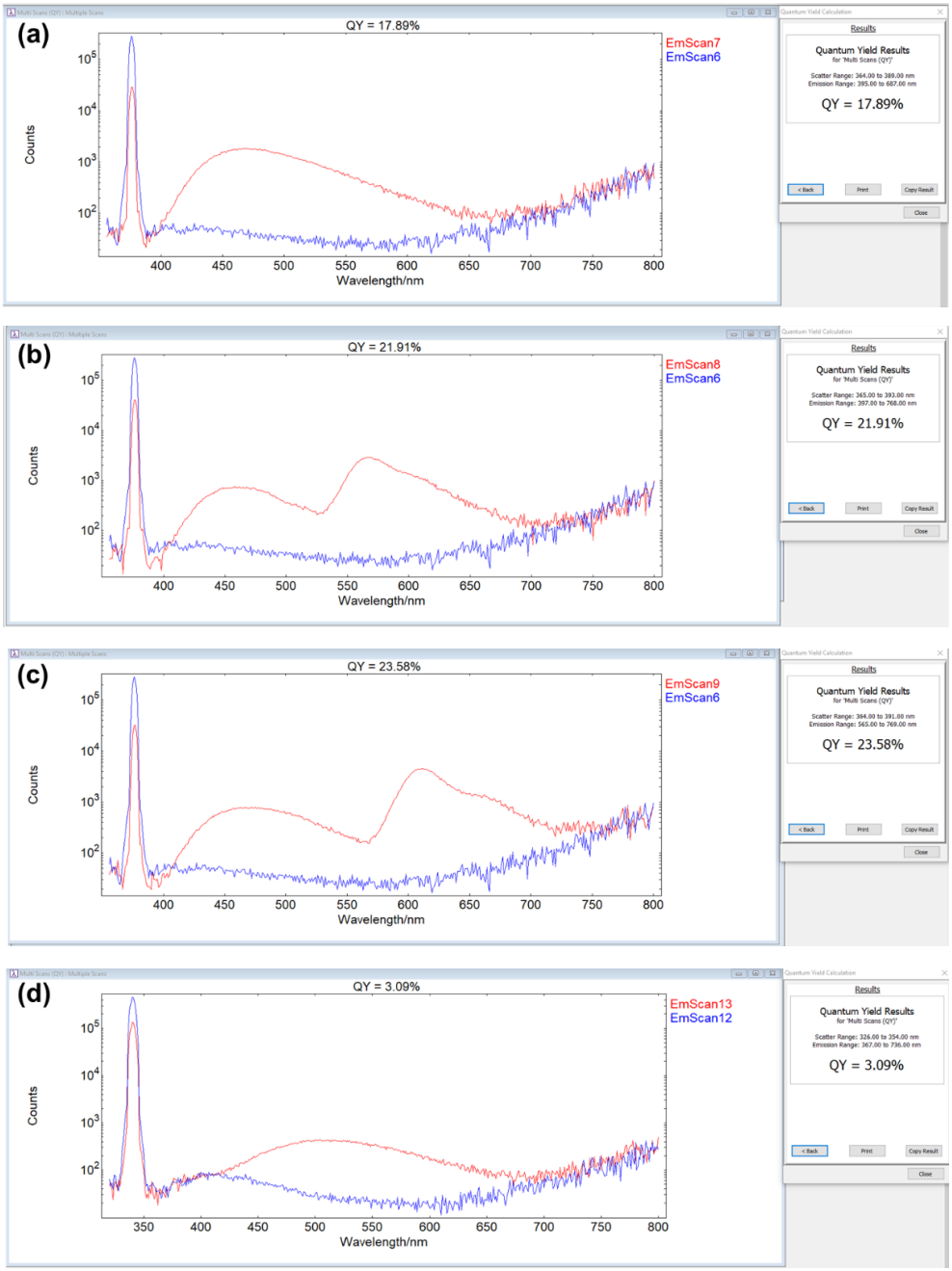

Figure S17. Fluorescence quantum yields of (a) **Zn-1**; (b) **Zn-1⊃EY** (2:1); (c) **Zn-1⊃SR101** (2:1) and (d) **L** upon excitation at 375 nm.

Table S3. Fluorescence quantum yields of **Zn-1**, **Zn-1⊃EY**, and **Zn-1⊃ SR101** in DMF solution.

Sample	Concentration	Fluorescence quantum yields Φ_F
Zn-1	[Zn-1] = 1.0×10^{-5} M	17.89%
Zn-1⊃EY	[Zn-1] = 1.0×10^{-5} M, [EY] = 5.0×10^{-6} M	21.91%
Zn-1⊃SR101	[Zn-1] = 1.0×10^{-5} M, [SR101] = 5.0×10^{-6} M	23.58%
L	[L] = 1.0×10^{-5} M	3.09%

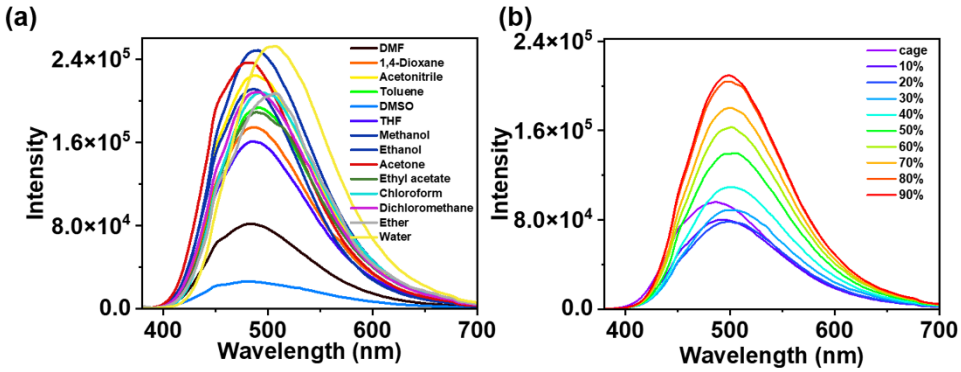

Figure S18. (a) Fluorescence spectra of **Zn-1** in different solvents (λ_{ex} = 375 nm, [Zn-1] = 1.0×10^{-5} M, DMF/ other solvent 1:99); (b) fluorescence emission spectra of **Zn-1** ([Zn-1] = 1.0×10^{-5} M) versus water fraction in DMF/water mixtures (λ_{ex} = 375 nm).

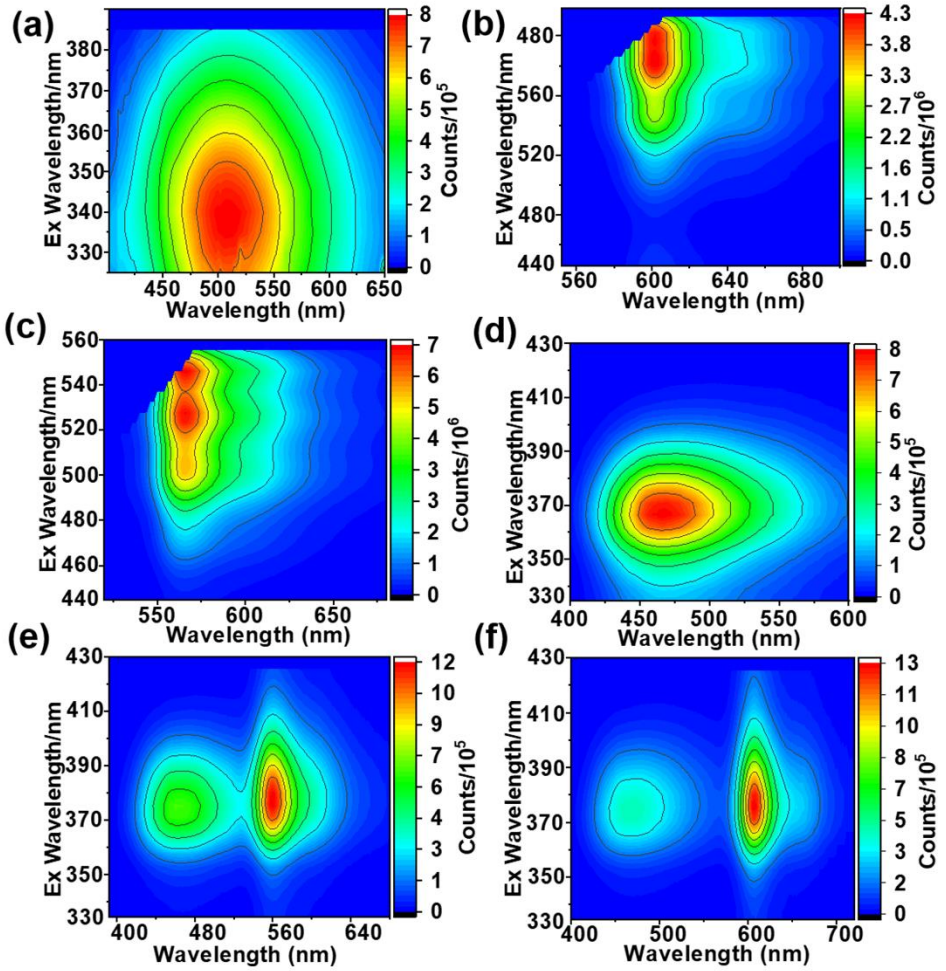

Figure S19. The 3D fluorescence spectrum of (a) **L**; (b) **Zn-1**; (c) **EY**; (d) **SR101**; (e) **Zn-1⊃EY**; (f) **Zn-1⊃SR101** upon different wavelengths excitation in DMF.

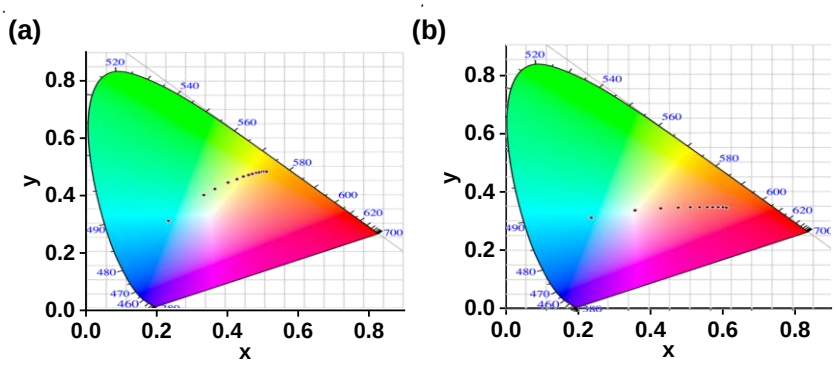

Figure S20. (a) The CIE chromaticity diagram changes of **EY** upon titration with **Zn-1** (0 to 0.6 equiv.); (b) the CIE chromaticity diagram changes of **SR101** upon titration with **Zn-1** (0 to 0.5 equiv.).

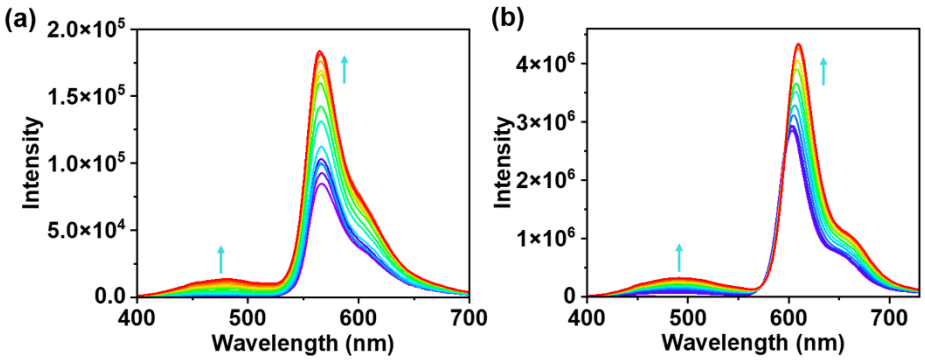

Figure S21. FRET process between **Zn-1** and **EY** (**SR101**). (a) fluorescence spectrum of **EY** ([EY] = 1.0×10^{-5} M) in DMF with different concentrations of **Zn-1** (λ_{ex} = 375 nm); (b) fluorescence spectrum of **SR101** ([SR101] = 1.0×10^{-5} M) in DMF with different concentrations of **Zn-1** (λ_{ex} = 375 nm).

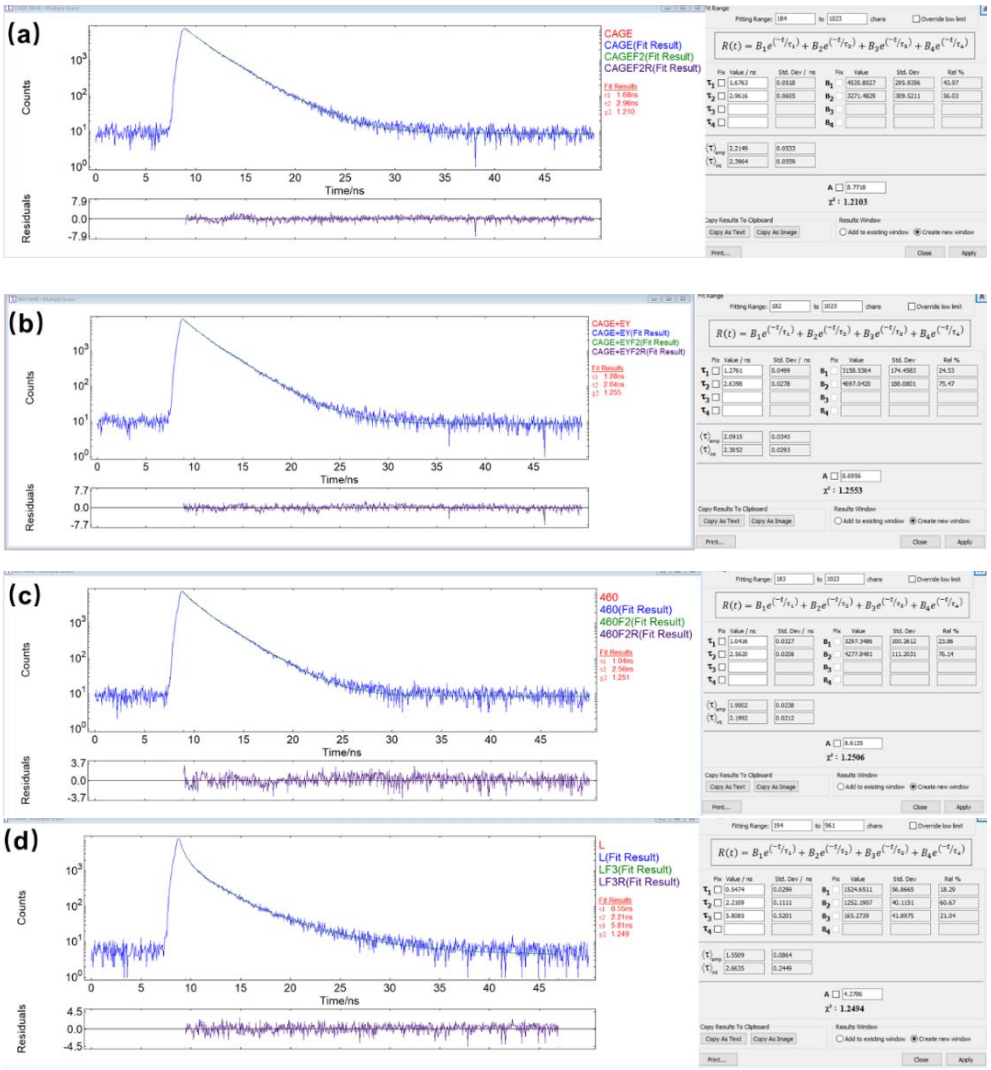

Figure S22. Fluorescence decay profile of (a) **Zn-1,** [Zn-1] = 1.0×10^{-5} M; (b) **Zn-1⊃EY** (2:1), [Zn-1] = 1.0×10^{-5} M, [EY] = 5.0×10^{-6} M; (c) **Zn-1⊃ SR101** (2:1) [Zn-1] = 1.0×10^{-5} M, [SR101] = 5.0×10^{-6} M; (d) **L** excitation at 375 nm, [L] = 1.0×10^{-5} M.

Table S4. Fluorescence lifetimes of **Zn-1**, **Zn-1⊃EY** and **Zn-1⊃ SR101** in DMF solution.

Sample	τ_1/ns	Rel%	τ_2/ns	Rel%	τ_{int}/ns	χ^2
Zn-1	1.6763	43.97	2.9616	56.03	2.3964	1.2103
Zn-1⊃EY	1.2761	24.53	2.6398	75.47	2.3052	1.2553
Zn-1⊃ SR101	1.0416	23.86	2.5620	76.14	2.1992	1.2506

Energy-transfer efficiency (Φ_{ET})

Energy-transfer efficiency (Φ_{ET}) was calculated from excitation spectra using equation.

$\Phi_{ET} = 1\text{-}I_{DA}/I_D$

Where I_{AD} is fluorescence intensity of the excitation of **Zn-1⊃EY** (**Zn-1⊃SR101**) in presence of **EY**(**SR101**), I_D is the fluorescence intensity of the excitation of **Zn-1**, respectively.

Table S5. Energy-transfer efficiency (Φ_{ET}) of **Zn-1⊃EY** and **Zn-1⊃ SR101** in DMF solution.

	λ_{ex}	I_{DA}	I_D	Φ_{ET}
Zn-1⊃EY	375nm	198023.266	1126074.75	82.41%
Zn-1⊃SR101	375nm	449871.375	878009.188	48.76%

Antenna effect

The antenna effect (AE) under certain concentrations of donor and acceptor equals the ratio of the emission intensity of the acceptor upon excitation of the donor, to that of the direct excitation of the acceptor. [S12]

Antenna effect was calculated from excitation spectra using equation.

$$AE = \frac{I_{AF\lambda(AD,375)} - I_{AF\lambda(D,375)}}{I_{AF\lambda(A,485)}}$$

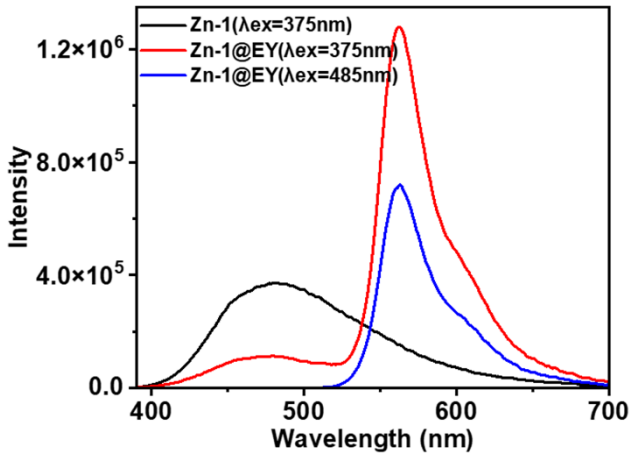

Figure S23. Fluorescence emission intensity of **Zn-1** (λ_{ex} = 375 nm), **Zn-1⊃EY** ([Zn-1] = 1.0 × 10^{-5} M, [EY] = 6.0 × 10^{-6} M, λ_{ex} = 375 nm) and **Zn-1⊃EY** ([Zn-1] = 1.0 × 10^{-5} M, [EY] = 6.0 × 10^{-6} M, λ_{ex} = 485 nm).

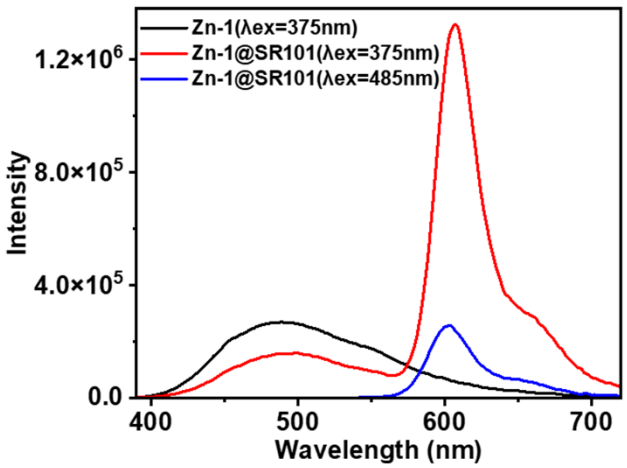

Figure S24. Fluorescence emission intensity of **Zn-1** (λ_{ex} = 375 nm), **Zn-1⊃SR101** ([Zn-1] = 1.0 × 10^{-5} M, [SR101] = 5.5× 10^{-6} M, λ_{ex} = 375 nm) and **Zn-1⊃SR101** ([Zn-1] = 1.0 × 10^{-5} M, [SR101] = 5.5× 10^{-6} M, λ_{ex} = 485 nm).

The antenna effect value for the **Zn-1⊃EY** and **Zn-1⊃ SR101** were calculated as 1.5 and 5.6 in DMF solution.

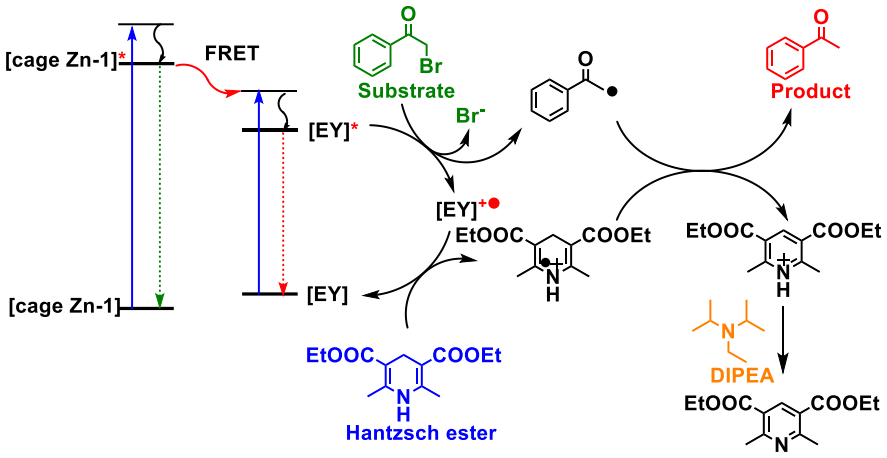

Figure S25. Proposed reaction pathways of the dehalogenation reaction using **Zn-1⊃EY** as photocatalyst.

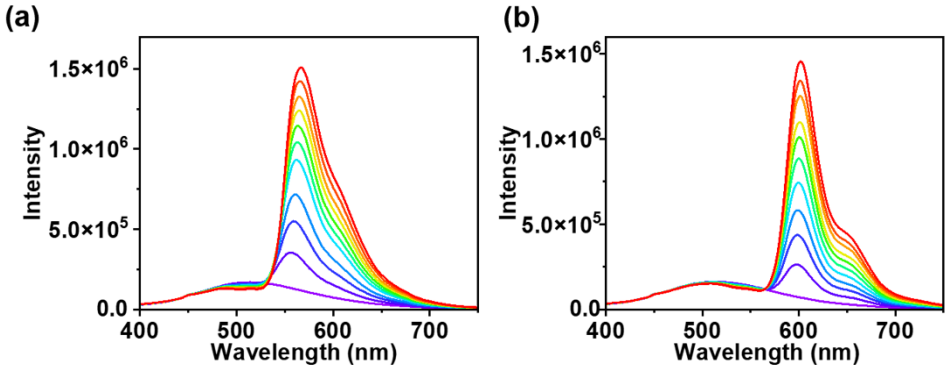

Figure S26. Almost any FRET process between **L** and **EY**/**SR101**. (a) fluorescence spectrum of **L** ([L] = 1.0 × 10^{-5} M) in DMF with different concentrations of **EY**; (b) fluorescence spectrum of **L** ([L] = 1.0 × 10^{-5} M) in DMF with different concentrations of **SR101**.

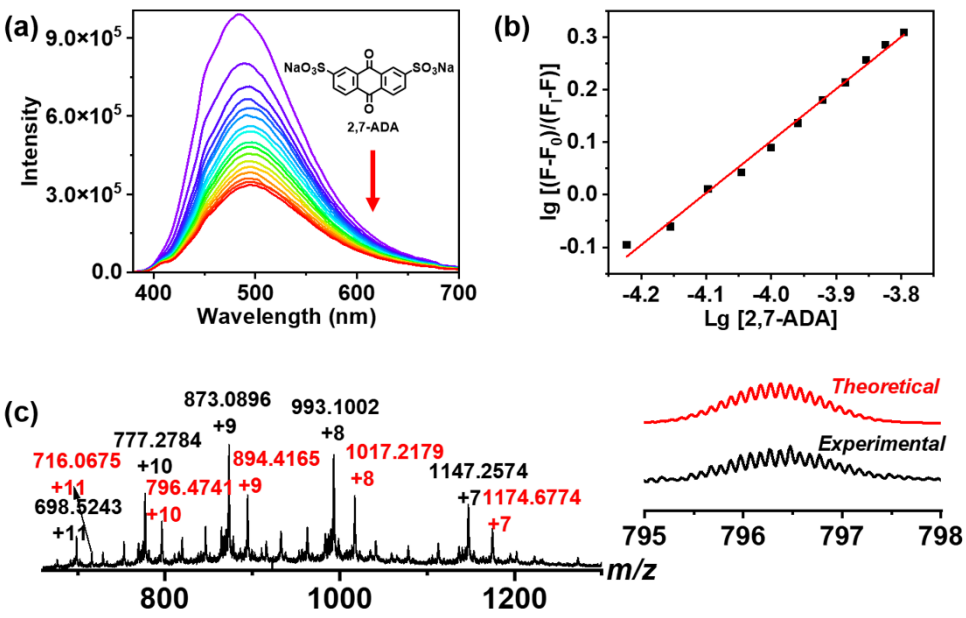

Figure S27. (a) Family of luminescence spectra of **Zn-1** ([Zn-1] = 1.0 × 10^{-5} M) in DMF upon the addition of 2,7-ADA; (b) Hill-plot of titration curve showing the calculation of the association constant (K = 1.2× 10^{5} M^{-1}); (c) ESI-MS spectra of **Zn-1**⊃2,7-ADA; experimental and calculated peak for **Zn-1**⊃2,7-ADA.

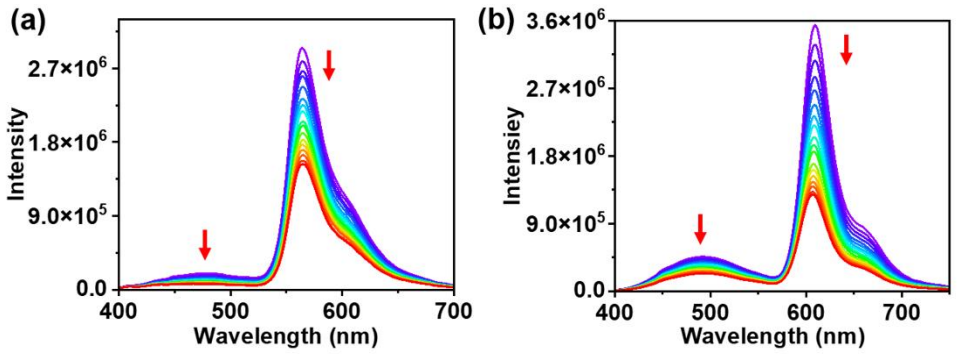

Figure S28. Prevent the FRET process by binding a competing guest in the host **Zn-1** (a) family of luminescence spectra of **Zn-1⊃EY** ([Zn-1] = 1.0 × 10^{-5} M, [EY] =6.0 × 10^{-6} M) in DMF upon the addition of 2,7-ADA; (b) family of luminescence spectra of **Zn-1⊃SR101** ([Zn-1] = 1.0 × 10^{-5} M, [SR101] =5.0 × 10^{-6} M) in DMF upon the addition of 2,7-ADA.

6 Supplemental References

S1: Serra-Pont, A.; Alfonso, I.; Solã, J.; Jimeno, C. An efficient dynamic asymmetric catalytic system within a zinc-templated network. Chem. Commun., 2019, 55, 7970-7973.

S2: Shustova, N. B.; McCarthy, B. D.; Dincå, M. Turn-On Fluorescence in Tetraphenylethylene-Based Metal–Organic Frameworks: An Alternative to Aggregation-Induced Emission. J. Am. Chem. Soc. 2011, 133, 20126-20129.

S3: SMART Data collection software, version 5.629, Bruker AXS Inc., Madison, WI, 2003.

S4: SAINT Data reduction software, version 6.45, Bruker AXS Inc., Madison, WI, 2003.

S5: G. M. Sheldrick, SHELX-97, Program for Crystal Structure Analysis (University of Göttingen: Göttingen, Germany, 1997).

S6: Stewart, J. J. P. Optimization of parameters for semiempirical methods VI: more modifications to the NDDO approximations and re-optimization of parameters. J. Mol. Model. 2013, 19, 1-32.

S7: Frisch, M. J.; Trucks, G. W.; Schlegel, H. B.; Scuseria, G. E.; Robb, M. A.; Cheeseman, J. R.; Scalmani, G.; Barone, V.; Petersson, G. A.; Nakatsuji, H.; Li, X.; Caricato, M.; Marenich, A. V.; Bloino, J.; Janesko, B. G.; Gomperts, R.; Mennucci, B.; Hratchian, H. P.; Ortiz, J. V.; Izmaylov, A. F.; Sonnenberg, J. L.; Williams; Ding, F.; Lipparini, F.; Egidi, F.; Goings, J.; Peng, B.; Petrone, A.; Henderson, T.; Ranasinghe, D.; Zakrzewski, V. G.; Gao, J.; Rega, N.; Zheng, G.; Liang, W.; Hada, M.; Ehara, M.; Toyota, K.; Fukuda, R.; Hasegawa, J.; Ishida, M.; Nakajima, T.; Honda, Y.; Kitao, O.; Nakai, H.; Vreven, T.; Throssell, K.; Montgomery Jr., J. A.; Peralta, J. E.; Ogliaro, F.; Bearpark, M. J.; Heyd, J. J.; Brothers, E. N.; Kudin, K. N.; Staroverov, V. N.; Keith, T. A.; Kobayashi, R.; Normand, J.; Raghavachari, K.; Rendell, A. P.; Burant, J. C.; Iyengar, S. S.; Tomasi, J.; Cossi, M.; Millam, J. M.; Klene, M.; Adamo, C.; Cammi, R.; Ochterski, J. W.; Martin, R. L.; Morokuma, K.; Farkas, O.; Foresman, J. B.; Fox, D. J. Gaussian 16 Rev. A.03, Wallingford, CT, 2016.

S8: Collins, J. B.; Schleyer, P. V.; Binkley, J. S.; Pople, J. A. Self-consistent molecular orbital methods. XVII. Geometries and binding energies of second-row molecules. A comparison of three basis sets. J. Chem. Phys. 1976, 64, 5142-5151.

S9: Hehre, W. J.; Stewart, R. F.; Pople, J. A. Self-Consistent Molecular-Orbital Methods. I. Use of Gaussian Expansions of Slater-Type Atomic Orbitals. J. Chem. Phys. 1969, 51, 2657-2664.

S10: Becke, A. D. Density-functional thermochemistry. III. The role of exact exchange. J. Chem. Phys. 1993, 98, 5648-5652.

S11: Lee, C. T.; Yang, W. T.; Parr, R. G. Development of the Colle-Salvetti Correlations-energy Formula into a Functional of the Electron-density. Phys. Rev. B 1988, 37, 785-789.

S12: Hao, M.; Sun, G.; Zuo, M.; Xu, Z.; Chen, Y.; Hu, X.; Wang, L. A Supramolecular Artificial Light-Harvesting System with Two-Step Sequential Energy Transfer for Photochemical Catalysis. Angew. Chem., Int. Ed., 2020, 59, 10095-0100.